J. Fluid Mech. (1981), *vol.* 109, *pp.* 259–275
Printed in Great Britain

Three-dimensional flow in a closed thermosyphon

By G. D. MALLINSON, A. D. GRAHAM
Department of Defence, Defence Science and Technology Organisation, Aeronautical Research Laboratories, Melbourne, Australia
AND G. DE VAHL DAVIS
University of New South Wales, Sydney, Australia

(Received 5 September 1980 and in revised form 28 January 1981)

A numerical and experimental study has been made of the three-dimensional flow and heat transfer by natural convection in a closed, rectangular thermosyphon. At low Rayleigh numbers, the flows in the two halves of the cavity remain separate, with heat transfer across the mid-height plane occurring only by conduction. At increasing Rayleigh numbers, an exchange process of increasing complexity occurs. The numerical solutions were used to explore this process and to predict flow patterns which were found to resemble closely those observed during previous investigations of cylindrical thermosyphons. The results were verified by a flow visualization study. Heat-transfer rates are presented and augment previous data for higher values of the governing parameters.

1. Introduction

A closed thermosyphon is a long cylindrical cavity, often of circular cross-section, the walls of the lower half of which are maintained at a higher temperature than the walls of the upper half. (In this paper, only stationary, vertical thermosyphons have been considered.) These thermal conditions create an unstable stratification near the region of the mid-height of the cylinder. In the upper half of the cylinder, the fluid moves so that it descends near the walls and ascends near the vertical axis; in the lower half, it descends near the axis and ascends near the walls. If the motion is sufficiently strong, the downwards flow near the walls of the upper half of the cylinder feeds the flow near the axis of the lower half, while the flow near the axis of the upper half is fed from the wall layers of the lower half. A complex three-dimensional exchange process is thus established in the mid-height region.

The closed thermosyphon has practical application in the cooling of turbine blades (Ogale 1968, an application in which the device is not stationary and vertical) and in the preservation of permafrost beneath buildings in ice-bound regions such as the Canadian northland (Larkin 1967).

Japiske & Winter (1970) and Japiske, Jallouk & Winter (1971) performed a detailed experimental study of a closed thermosyphon with a circular horizontal cross-section. In terms of the Prandtl number, Pr, and a parameter t_{ct} ($= 2Ra/h$, where Ra is the Rayleigh number based on the diameter of the cross-section and h is the vertical aspect ratio), they made the following general observations.

For $t_{ct} \lesssim 10^7$ the exchange process is laminar and consists of individual streams of

ascending hot and descending cold fluid crossing the mid-height plane. The number of streams increases with t_{ct}. For example four streams (two up and two down) were observed when $t_{ct} \simeq 10^4$, six streams when $10^5 \lesssim t_{ct} \lesssim 5 \times 10^5$ and as many as 10 streams when $t_{ct} \simeq 1{\cdot}5 \times 10^6$. Generally the flow is steady for $Pr > 90$ and unsteady for $Pr < 20$ although as t_{ct} increases a tendency for the streams to drift with time develops so that a stable steady state exists only for $Pr > 90$ and $t_{ct} \lesssim 5 \times 10^5$.

For the stronger laminar flows ($t_{ct} \gtrsim 10^5$) heat is transferred across the mid-height plane predominantly by convection. For $t_{ct} > 10^7$ the flow is turbulent and heat is transferred by a mixing process.

These observations indicate that the flow and heat transfer should be amenable to a steady-state laminar numerical analysis for $Pr > 90$ and $0 \leqslant t_{ct} \leqslant 5 \times 10^5$. The challenge to such an analysis is that the flow field in the thermosyphon is fully three-dimensional: it cannot even be regarded as a perturbation of a two-dimensional flow as is, for example, the flow field in the heated cavity studied by Mallinson & de Vahl Davis (1977).

This paper presents the results of such a numerical analysis. To reduce computational expenditure, the numerical solutions are for a cavity of square (rather than circular) cross-section. These solutions are shown to be in favourable agreement with both the Japikse & Winter (1970) and Japikse *et al.* (1971) experiments and a flow visualization study we have made of a square cross-section thermosyphon. Heat-transfer results for $0 \leqslant t_{ct} \leqslant 4 \times 10^5$ are presented and augment the existing data of Japiske *et al.* for $t_{ct} \geqslant 5 \times 10^5$.

2. Mathematical formulation and solution method

The mathematical formulation of the equations of motion and their method of solution have been described previously (Mallinson & de Vahl Davis 1973, 1977). In brief, we considered the motion of a fluid in a rectangular box of dimensions L, L and hL in the x, y and z directions respectively; the z axis is directed vertically downwards. The Boussinesq (1903) approximation was made, and the fluid properties were otherwise treated as being constant. The motion was assumed to be laminar and steady. The non-dimensional equations for the vector potential $\bar{\Psi}$, vorticity $\bar{\zeta}$ and temperature θ are

$$\bar{\zeta} = -\nabla^2 \bar{\Psi}, \tag{1}$$

$$Pr^{-1}(\nabla \times (\bar{\zeta} \times \bar{v})) = -Ra(\nabla \times \theta \bar{k}) + \nabla^2 \bar{\zeta}, \tag{2}$$

$$\nabla . (\bar{v}\theta) = \nabla^2 \theta, \tag{3}$$

where $\bar{v}$ denotes velocity and $\bar{k}$ is the unit vector in the z direction;

$$Ra = g\beta(T_h - T_c)\, L^3/\kappa\nu \quad \text{and} \quad Pr = \nu/\kappa$$

are the Rayleigh and Prandtl numbers; β, κ and ν are the coefficients of volumetric expansion, thermal diffusivity and kinematic viscosity; L, L^2/κ and κ/L have been used as scale factors for length, time and velocity; θ is related to the dimensional temperature T by $\theta = (T - T_c)/(T_h - T_c)$; g is the gravitational acceleration; and T_h and T_c are the (dimensional) wall temperatures in the lower and upper halves of the box respectively.

Remembering that z is directed downwards, the boundary conditions for θ are:

$$\theta = 0 \quad \text{for} \quad z \leqslant \tfrac{1}{2}h - \Delta z; \tag{4}$$

$$\theta = \frac{z - h/2 + \Delta z}{2\Delta z} \quad \text{for} \quad |z - \tfrac{1}{2}h| < \Delta z; \tag{5}$$

$$\theta = 1 \quad \text{for} \quad z \geqslant \tfrac{1}{2}h + \Delta z. \tag{6}$$

The length Δz is the mesh interval in the z direction. Equation (5) limits the thermal gradient in the mid-height region of the thermosyphon walls. In reality this limit is imposed by the thermal properties of the walls; numerically it is imposed by Δz. Note that conditions (4) and (6) imply that the $z = 0$ and $z = h$ boundaries are isothermal, whereas the experimental cavity used by Japiske and his co-workers (1970, 1971) had ends that were nearly adiabatic.

The conditions on $\bar{\Psi}$ at each boundary are that $\bar{\Psi}$ is normal to the boundary and that the normal derivative of its normal component is zero. The conditions on $\bar{\zeta}$ are that its normal component is zero and each tangential component is given by

$$\zeta_s = -\partial^2 \psi_s / \partial s^2, \tag{7}$$

where ζ_s and ψ_s are the components of $\bar{\zeta}$ and $\bar{\Psi}$ in the s (tangential) direction.

A set of finite-difference equations was generated by replacing all the derivatives in the governing equations (1)–(3) and the boundary conditions (7) by second-order central difference approximations in such a way that conservation was preserved (Mallinson & de Vahl Davis 1973). Transient terms, chosen to speed the approach to steady state, were added to these equations and approximated by first-order forward differences. The whole system was solved by an alternating direction implicit solution procedure, the final steady state being the solution of the original equations (1)–(3).

Initial conditions for each solution were either 'rest' conditions, with $\bar{v} = 0$ and $\theta = 0{\cdot}5$ throughout the fluid, or a previously converged solution. In either case the initial state could be disturbed by adding values, randomly selected from the interval (0·25, 0·75), to the central half of the θ field during the first iteration of the solution process. A solution was considered to be converged when the sums of the absolute changes in $\bar{\zeta}$, $\bar{\Psi}$ and θ normalized by selected values of the appropriate quantities were less than 10^{-5}. This convergence test was augmented by a careful examination of solution transients.

Once a steady-state solution was obtained a Nusselt number Nu, representing heat transfer across the mid-height plane, was computed by evaluating

$$Nu_{i,j} = (\theta_{i,j,k_m+1} - \theta_{i,j,k_m-1})/2\Delta z - (w\theta)_{i,j,k_m} \tag{8}$$

at each (i, j) mesh point in the mid-height plane ($k = k_m$). A double application of Simpson's rule was then used to estimate

$$Nu = \int_0^1 \int_0^1 \left(\frac{\partial \theta}{\partial z} - w\theta\right)\Big|_{z=\frac{1}{2}h} dx\, dy. \tag{9}$$

Numerical experiments indicated that the solutions were Pr independent if $Pr \geqslant 10^2$. Solutions were obtained for $h = 1$, 2 and 4 for $10^3 \leqslant Ra \leqslant 2 \times 10^5$ (or $5 \times 10^2 \leqslant t_{ct} \leqslant 4 \times 10^5$) and are valid for all $Pr \geqslant 10^2$.

The mesh sizes used were $15 \times 15 \times 15$ for $h = 1$, $15 \times 15 \times 21$ for $h = 2$ and $11 \times 11 \times 41$ for $h = 4$. A compromise between accuracy and computing cost is always necessary. A limited exploration of mesh size effects in this three-dimensional study showed that no essential feature of the flow has been suppressed in the solutions presented here. More extensive studies which we have made of the effects of mesh size in two-dimensional flow suggest that the Nusselt numbers given below will be in error by no more than about 5 per cent.

3. Experimental flow visualization technique

The experimental investigation was limited to $h = 2$ and used the square cross-section thermosyphon described by Mallinson & Graham (1974). This consisted of a box within a box, the inner box forming a $76 \times 76 \times 152$ mm test cavity. The space between the two boxes was divided by a spacer at the plane $z = \frac{1}{2}h$ to form two water jackets which were fed from constant temperature baths, the water flow rate from which was sufficient to ensure that the spatial temperature variation of the water in the jackets was less than 0·05 K. To retain a maximum degree of visibility, the whole apparatus was constructed from Perspex. The walls of the innermost box were kept as thin as possible (3 mm), subject to strength requirements, to reduce thermal gradients and subsequent departures from the ideal 'isothermal' boundary conditions.

Silicone oils of several viscosity grades, ranging from 5×10^{-4} to $1{\cdot}25 \times 10^{-2}$ m^2 s^{-1}, were used as working fluids in the thermosyphon. For $3 < (T_h - T_c) < 50$ K the accessible Rayleigh-number range was from 10^4 to 5×10^6. For the grades of oil used,

$$5 \times 10^3 \leqslant Pr \leqslant 10^5,$$

so that the experiments can be compared directly with the numerical solutions.

The motion of the oil was rendered visible by neutrally buoyant particles which were produced from beeswax. The wax was melted and impregnated with a small amount of fluorescent paint pigment which increased the reflectivity of the particles and provided some control of their final specific gravity. After solidification the wax was ground and sieved to produce particles with diameters in the range 0·2–1 mm. Particles were then introduced into a volume of oil and allowed to settle for 24 h before the oil was poured into the cavity, thus providing a final selection of neutrally buoyant particles.

The particles were illuminated by a collimated 5 mm thick sheet of light produced by a 150 W halogen low-voltage source and a system of lenses and slits. The most meaningful pictures were obtained when the sheet was perpendicular to one of the co-ordinate axes used in the numerical model. The majority of flow visualization photographs are slices in the vertical x or y planes. A limited number of z slices were photographed using a mirror placed underneath the thermosyphon. However, poor visibility in this direction meant that the success rate was relatively low.

4. Conduction regime ($Ra \leqslant 10^3$)

Whereas Japiske and co-workers (1970, 1971) used t_{ct} to classify their observations (which were based on a single aspect ratio of 8), the present numerical results indicate that the Rayleigh number is better for delineating the various flow regimes. For

$Ra \lesssim 10^3$ the flow is weak and heat is transferred across the mid-height plane by conduction. For $Ra > 10^3$ convection across the mid-height plane makes an increasing contribution to the heat transfer.

4.1. *Fluid motion*

Although fluid motion occurs for any non-zero Rayleigh number, convection across the mid-height plane exists only when the Rayleigh number exceeds a critical value, Ra_c. For $1 \leqslant h \leqslant 4$, the numerical solutions indicate that $10^3 < Ra_c < 5 \times 10^3$. Our experiments were limited to $Ra \geqslant 10^4$ and could not provide an estimate for Ra_c.

When $Ra < Ra_c$ the flow has the form illustrated in figure 1 (*a*) by streamlines in the planes $x = 0{\cdot}5$ and $y = 0{\cdot}5$ of a solution with $h = 2$ and $Ra = 10^3$. In these planes of symmetry, the flow is two-dimensional and the streamlines close. They appear to be part of a flow field that consists of two counter-rotating vortex rings as indicated by the vortex lines also shown in figure 1 (*a*). The vortex lines near the axis of the flow are almost circular in plan despite the square cross-section of the cavity.

If the cavity had been circular in horizontal cross-section, the flow field would have been axisymmetrical and the vortex lines would have been precisely circular in plan. However, the fact that the cross-section is square means that the vortex lines are distorted; a non-axisymmetric circumferential motion is established, the net effect of which is illustrated by the streamline in figures 1 (*b*) and 1 (*c*). This streamline was traced from a point near the diagonal vertical plane through the origin. It spirals inwards, then moves towards the $y = 0{\cdot}5$ plane, where it spirals outwards before returning to the diagonal plane via the boundary layers. For clarity, this last return section has been omitted from figure 1 (*c*). Each vortex ring is composed of eight distinct flow regions bounded by the four vertical planes of symmetry. In each region the flow is completely self-contained and the streamlines are closed within the region.

4.2. *Heat transfer*

For $Ra = 0$, θ satisfies

$$\nabla^2\theta = 0, \tag{10}$$

subject to the boundary conditions (4)–(6). The solution can be written in the form

$$\theta = 0{\cdot}5 + \phi_x + \phi_y + \phi_z, \tag{11}$$

where ϕ_x satisfies (10) and the boundary conditions (4)–(6) on the $x = 0$ and $x = 1$ boundaries but is zero on all other boundaries. ϕ_y and ϕ_z similarly satisfy (10) and the non-homogeneous boundary conditions on the y and z boundaries respectively. Series expansions for the ϕ's can then be found, *viz.*

$$\phi_x = \frac{4}{\pi^2}\sum_{i=1}^{\infty}\sum_{j=1}^{\infty}\left[\frac{\sin\lambda_j}{\lambda_j} + (-1)^{j-1}\right]\frac{\sinh\lambda_{ij}(1-x) + \sinh\lambda_{ij}x}{(2i-1)j\sinh\lambda_{ij}}\sin(2i-1)\pi y\sin\lambda_j\frac{z-\frac{1}{2}h}{\Delta z}, \tag{12}$$

$$\phi_y = \frac{4}{\pi^2}\sum_{i=1}^{\infty}\sum_{j=1}^{\infty}\left[\frac{\sin\lambda_j}{\lambda_j} + (-1)^{j-1}\right]\frac{\sinh\lambda_{ij}(1-y) + \sinh\lambda_{ij}y}{(2i-1)j\sinh\lambda_{ij}}\sin(2i-1)\pi x\sin\lambda_j\frac{z-\frac{1}{2}h}{\Delta z}, \tag{13}$$

$$\phi_z = \frac{8}{\pi^2}\sum_{i=1}^{\infty}\sum_{k=1}^{\infty}\frac{\sin(2i-1)\pi x\sin(2k-1)\pi y\sinh\lambda_{ik}(z-\frac{1}{2}h)}{(2i-1)(2k-1)\sinh\lambda_{ik}}, \tag{14}$$

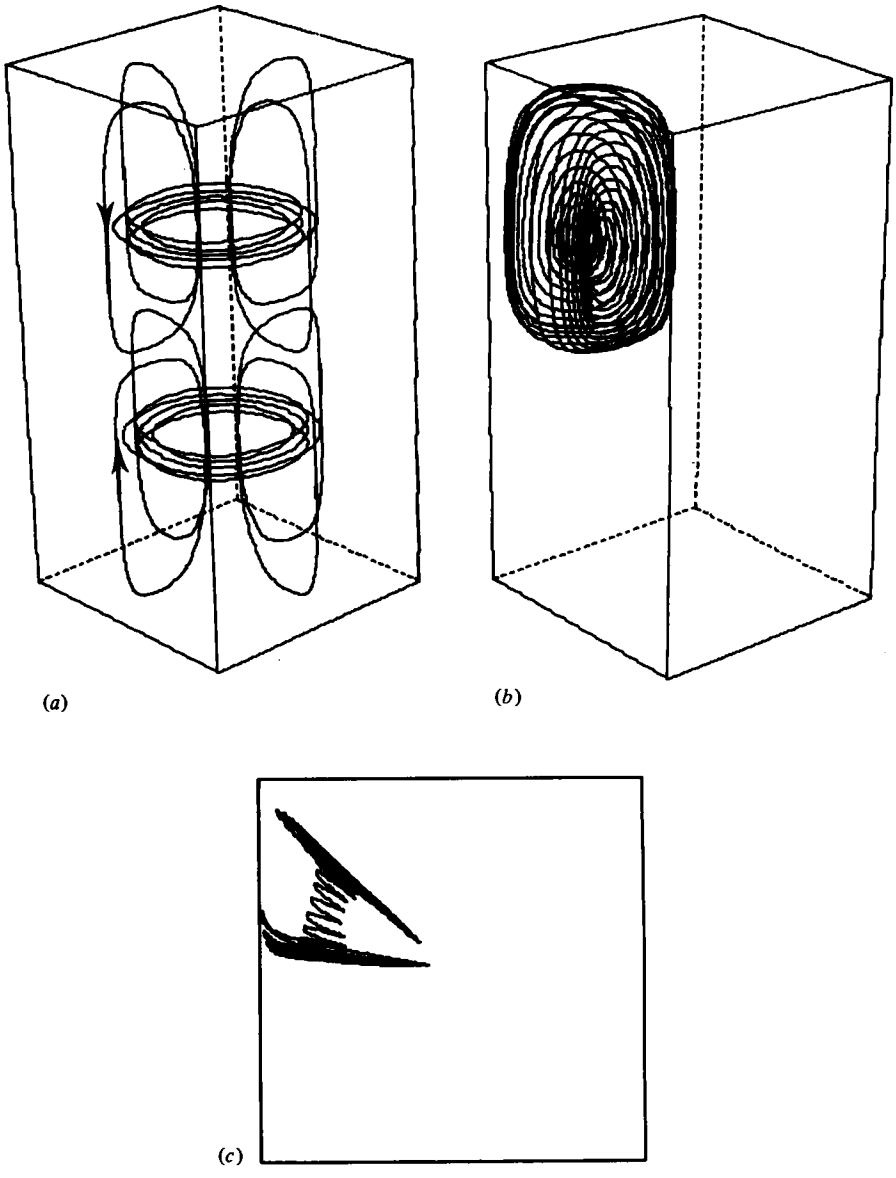

FIGURE 1. Flow in a thermosyphon with $h = 2$ and $Ra = 10^3$. (*a*) Streamlines in the $x = 0{\cdot}5$ and $y = 0{\cdot}5$ planes and vortex rings. (*b*) Streamline showing the effect of cavity geometry. (*c*) Plan view of portion of the streamline in (*b*).

where

$$\lambda_{ij}^2 = \pi^2[(2i-1)^2+(2j/h)^2], \quad \lambda_{ik}^2 = (h\pi/2)^2[(2i-1)^2+(2k-1)^2]$$

and

$$\lambda_j = (2j\pi\Delta z)/h.$$

Note that the solution depends on the mesh interval Δz, or the assumed thermal gradient maintained in the walls at the cavity mid-height. Although a solution can be found for the case of a perfect discontinuity across the mid-height, the series is not

h	Mesh size	Δz	Nu (series)	Nu (numerical)
1	$15 \times 15 \times 15$	0·071	2·98	2·98
2	$15 \times 15 \times 21$	0·1	2·53	2·51
4	$11 \times 11 \times 41$	0·1	2·53	2·54

TABLE 1. Flux estimates for $Ra = 0$ (series) and $Ra = 10^3$ (numerical).

absolutely convergent throughout the cavity and cannot be manipulated to yield the heat flux as in the following analysis.

The heat flux across the mid-height plane is given by

$$Nu = \int_0^1 \int_0^1 \left(\frac{\partial \phi_x}{\partial z} + \frac{\partial \phi_y}{\partial z} + \frac{\partial \phi_z}{\partial z} \right)_{z=\frac{1}{2}h} dx\, dy. \tag{15}$$

The series in equations (12)–(14) can be differentiated and integrated, term by term, to yield

$$Nu = \frac{64}{h\pi^2} \left\{ \sum_{i=1}^{\infty} \frac{1}{(2i-1)^2} \left[\sum_{j=1}^{\infty} \left(\frac{\sin \lambda_j}{\lambda_j} + (-1)^{j-1} \right) \frac{\coth \frac{1}{2}\lambda_{ij}}{\lambda_{ij}} + \sum_{k=1}^{\infty} \frac{\lambda_{ik}}{(2k-1)^2 \sinh \lambda_{ik}} \right] \right\}. \tag{16}$$

This series was evaluated for $h = 1$, 2 and 4 and the appropriate values of Δz. The three Nusselt numbers together with those estimated from numerical solutions at $Ra = 10^3$ are given in table 1. It is evident from these figures that convection has a negligible effect on the rate of heat transfer for $Ra \leqslant 10^3$.

An interesting observation is that the series solutions show that the effect of h on Nu is insignificant for $h \geqslant 2$. This observation was also supported by the temperature profiles along the vertical axis of the thermosyphon. The central half of the $h = 4$ profile was identical with the $h = 2$ profile. In fact for $h \geqslant 2$ the series representing ϕ_z can be neglected and the temperature field is determined entirely by the applied central gradient.

A corollary of this observation is that the toroidal flow is fixed in size for $h \geqslant 2$. Fluid outside $|z - \frac{1}{2}h| < 1$ is essentially stagnant.

5. Convection regime ($Ra > 10^3$)

5.1. *Fluid motion*

(a) Flow stability

For $Ra > Ra_c$, fluid crosses the mid-height plane and a convective exchange process is established. As observed by Japikse and co-workers (1970, 1971) the number of individual streams crossing the mid-height plane increases with Ra. There is a sequence of critical Rayleigh numbers at which the flow field undergoes transitions between configurations with differing numbers of streams.

A complete investigation of the stability of each flow configuration and a determination of every critical Rayleigh number would involve a prohibitive programme of numerical experiments. The observations made in this discussion are based on over 25 converged solutions each of which was obtained after imposing a disturbance on

either zero flow initial conditions or a previously converged solution for different parameter values and sometimes even a different flow configuration. The converged solutions are augmented by some 20 solution attempts in which the solution either failed to reach a steady state (indicating possible temporal instability of the flow) or, in the case of high Ra, became numerically unstable (indicating that the mesh was not capable of resolving a highly complicated flow configuration).

For $h = 2$, solutions were obtained for $Ra = 5 \times 10^3$, 10^4, 2×10^4, 3×10^4, 4×10^4, 5×10^4, 7×10^4, 10^5 and 2×10^5. Solutions for the other aspect ratios were obtained for some of these values and tended to concentrate on those values of Ra where transitions occurred for $h = 2$.

From these solutions, the following observations were made:

(i) The critical Rayleigh numbers for the transitions from two to four streams and four to six streams are in the ranges $(3\frac{1}{2}–4\frac{1}{2}) \times 10^4$ and $(1–2) \times 10^5$ respectively.

(ii) For Rayleigh numbers within the ranges given in (i) either transitional configuration could be obtained as a steady solution. Invariably the configuration with fewer streams convected more heat than the other configuration when Ra was near the lower end of the transition range; the opposite occurred when Ra was near the higher end. This suggests that the preferred mode of motion at a given Rayleigh number is the one which convects the more heat.

(iii) For Rayleigh numbers between these critical values and outside the transition ranges only one configuration was possible. The boundaries between the streams were located, where possible, along the diagonals of the mid-height plane.

(iv) For Rayleigh numbers such that two configurations were possible, the smaller aspect ratios admitted configurations with the boundary between streams located parallel to the walls of the thermosyphon. Often it was possible for the solution to oscillate slowly between the two types of alignment emulating the drift observed by Japikse & Winter (1970).

These observations were supported by the flow visualization study. When $Ra \lesssim 3 \times 10^4$ a weak but stable flow containing two streams could be generated. When $3 \times 10^4 < Ra < 5 \times 10^4$, the flow field was difficult to stabilize and tended to drift. A stable four-stream flow could be generated when $5 \times 10^4 \lesssim Ra \lesssim 10^5$, with six streams appearing when $Ra \gtrsim 1{\cdot}5 \times 10^5$. Beyond $Ra = 5 \times 10^5$ the flow became unsteady and turbulence developed near $Ra = 5 \times 10^6$.

(*b*) *Flow structure*

Experimentally the four-stream configuration for $5 \times 10^4 \lesssim Ra \lesssim 10^5$ was the most easily generated and was chosen for detailed analysis. A case study was made of the flow in a cavity with $Ra = 10^5$ and $h = 2$. Contour maps of θ in the planes $x = 0{\cdot}5$, $z = 0{\cdot}5$ and $z = 1$ are shown in figures 2(*a*), 2(*b*) and 2(*c*) respectively. The map of θ in the plane $z = 1$ identifies the four streams of fluid crossing the mid-height plane. Note the alignment of the boundaries between the streams. Two streams adjacent to the y boundaries carry hot fluid upwards and two adjacent to the x boundaries carry cold fluid downwards.

The contour map of θ in the $x = 0{\cdot}5$ plane indicates that in each half of the thermosyphon the temperature along the vertical axis is essentially constant. This fact was used by Japikse *et al.* (1971) to develop a boundary-layer heat-transfer model for

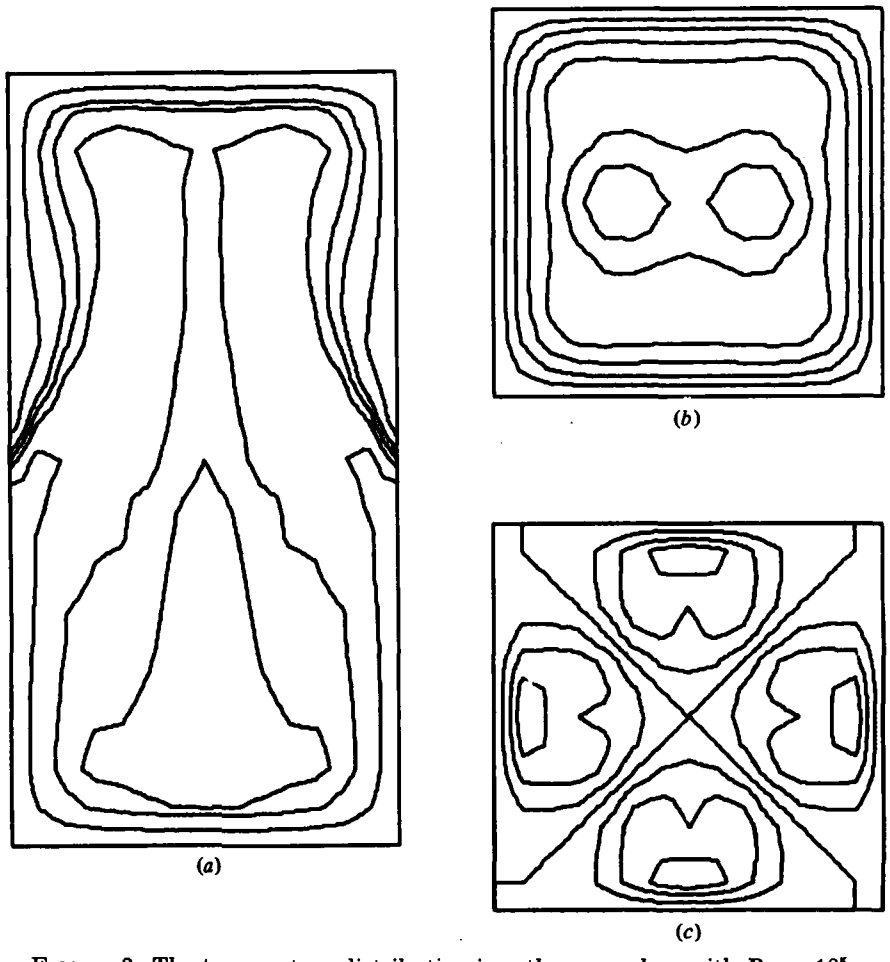

FIGURE 2. The temperature distribution in a thermosyphon with $Ra = 10^5$, in the planes (*a*) $x = 0{\cdot}5$, (*b*) $z = 0{\cdot}5$ and (*c*) $z = 1$.

$Ra > 5 \times 10^5$. Note, however, that the axial temperature is not representative of the bulk temperature of the coalesced streams (figure 2*b*).

Japikse *et al.* (1971) published a sketch of the flow at moderate Rayleigh numbers. This sketch showed the ascending and descending flows in the wall layers being deflected inwards near the mid-height plane. At some region of the cavity circumference, one flow would form a coherent stream and at the same region the opposing flow would be deflected back on itself to form a vortex. A similar diagram was constructed numerically by tracing streamlines which pass through points near the boundaries $x = 0$ and $y = 1$. In figure 3 (which has been hand-processed to remove hidden features) the cold fluid descending near the $x = 0$ boundary crosses the $z = 1$ plane as a stream and the rising hot fluid adjacent to the $y = 1$ boundary forms a similar stream. The formation of the vortices observed by Japikse *et al.* (1971) is clearly indicated.

The structure of the flow can, to some extent, be revealed by the flow visualization slices, which can also be simulated numerically to provide a means of verifying the numerical solutions. For a given steady-state solution, streamlines were traced,

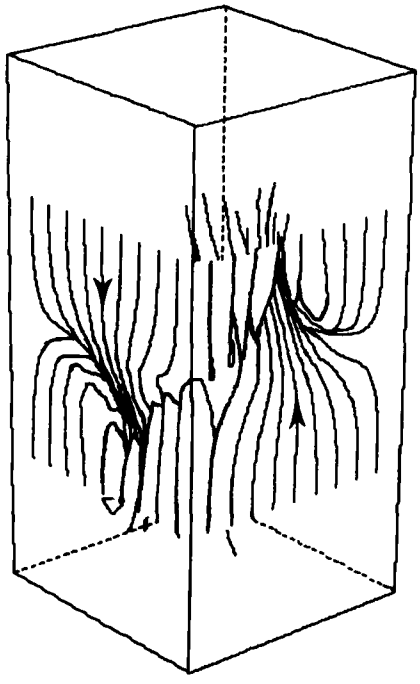

FIGURE 3. Flow near the walls in a thermosyphon with four streams; $Ra = 10^5$.

numerically, from points positioned at random in the space equivalent to that occupied by the 5 mm thick light beam. The streamlines were terminated when either the time interval of the photographic exposure was exceeded or the line left the confines of the beam. The number of points was chosen so that the simulation had a similar density of 'traces' to the photograph. Typically a simulation would contain around 200 streamlines. The results of simulations for the four-stream flow at $Ra = 7 \times 10^4$ are presented in figure 4 for three values of x and in figure 5 for two values of z.

The agreement between these simulations and the respective experimental visualizations is typical of that obtained throughout the range of parameter values studied. It should be noted that the construction of the experimental thermosyphon is such that approximately 5 mm at each end of the cavity is obscured from the camera. The solid white line on each photograph indicates the location of the cavity boundaries in the plane of the light beam.

The $x = 0{\cdot}5$ and $y = 0{\cdot}5$ planes are symmetry planes for the flow field. The slice at $x = 0{\cdot}5$ is shown in figure 4 (a, d). The direction of fluid flow is indicated in the photograph by a marker which was produced by extinguishing the beam for a short period immediately before the end of the exposure. The ascending streams near the y boundaries are clearly discernible, as are four centres of rotation. The streamlines in the plane do not close; the flow is not two-dimensional.

The two centres of rotation in the upper half of the plane are those of the vortices formed by the deflection upwards of the descending cold fluid adjacent to the y boundaries. In the lower half of the plane the fluid rotates as a result of the presence of the $z = 2$ boundary, which forces descending fluid near the vertical axis to feed the ascending wall layers.

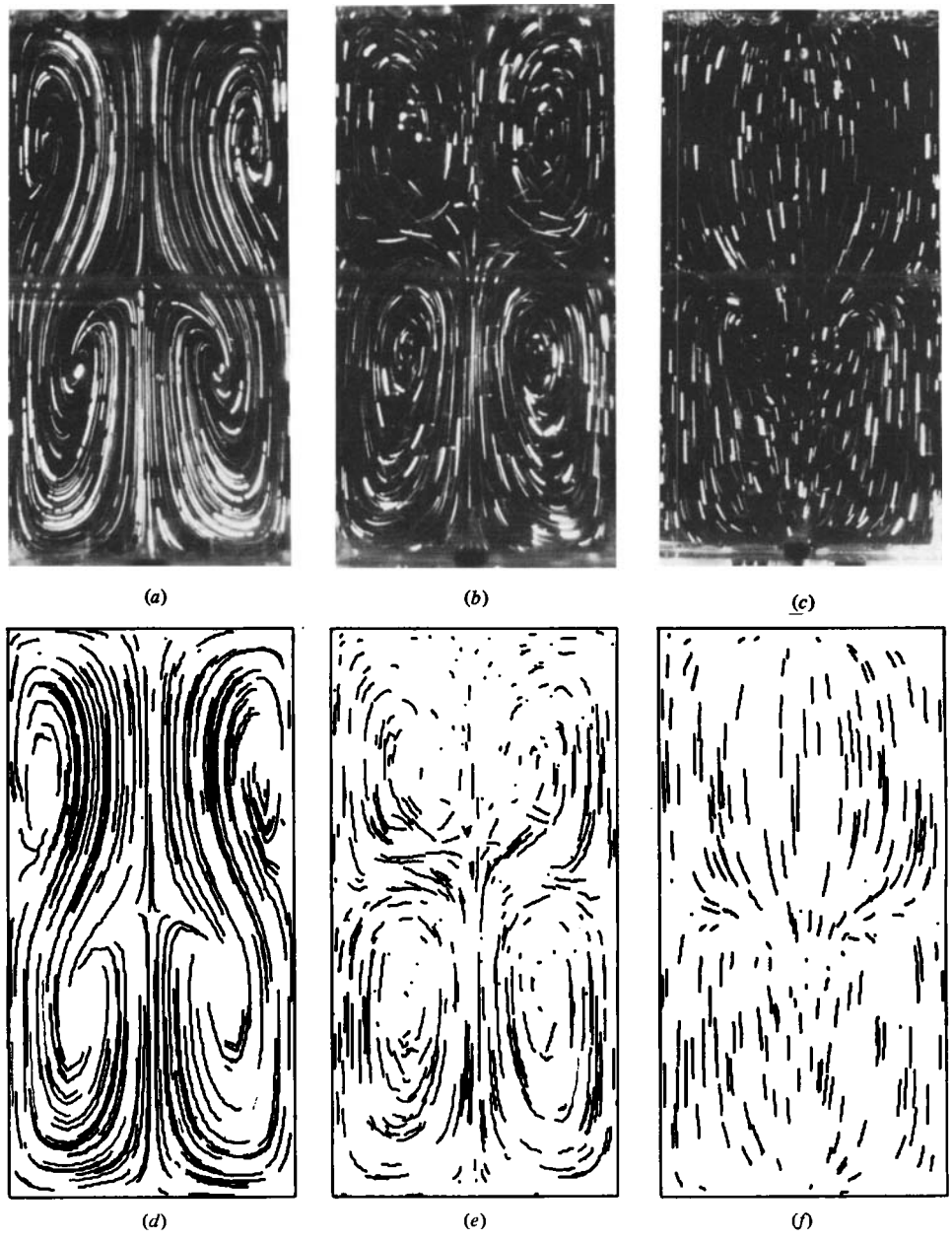

FIGURE 4. Flow visualizations (a, b, c) and numerical simulations (d, e, f); $Ra = 7 \times 10^4$. (a, d) beam centred on $x = 0{\cdot}5$ ($\Delta t = 5$ min); (b, e) beam centred on $x = 0{\cdot}25$ ($\Delta t = 2$ min); (c, f) beam adjacent to the $x = 0$ boundary ($\Delta t = 2$ min).

Flow in the plane $y = 0{\cdot}5$ is the same as the inverse with respect to z of that in the $x = 0{\cdot}5$ plane. The various centres of rotations in these symmetry planes belong to two stretched vortex rings. The ring in the upper half of the thermosyphon is stretched in the y direction; that in the lower half is stretched in the x direction. This is confirmed by the $x = 0{\cdot}25$ slice which has cut the upper ring in the direction of stretch.

Figures 4 (b, e) illustrate one of the consequences of the use of a relatively thick

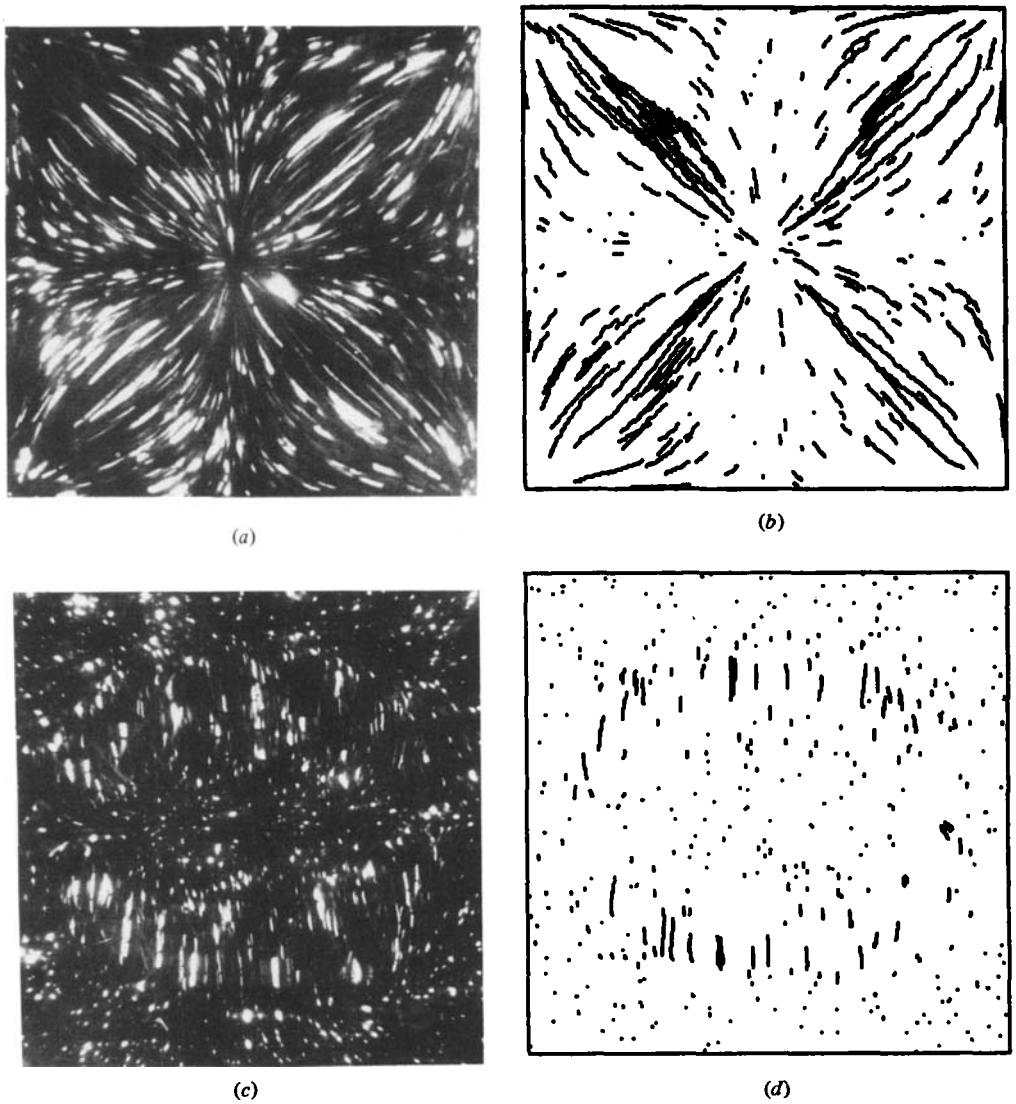

FIGURE 5. Flow visualizations (a, c) and numerical simulations (b, d); $Ra = 7 \times 10^4$. (a, b) beam centred on $z = 1{\cdot}0$ ($\Delta t = 5$ min); (c, d) beam centred on $z = 0{\cdot}5$ ($\Delta t = 5$ min).

beam (7 % of the cavity width): some streamlines appear to cross each other. Such streamlines are not coplanar. The use of a thinner beam would have avoided this to some extent, but would have led to the appearance of fewer and shorter streamlines in the photographs and simulations. The shorter tracks in figures 4(b, e) are due in part to the shorter exposure used, but also to the fact that the motion near $x = 0{\cdot}25$ is not predominantly *in* that plane (as it is at $x = 0{\cdot}5$), but *across* the plane, so that particles enter and leave the illuminated region during the exposure.

The slice near the $x = 0$ wall, figure 4(c, f), can be compared with figure 3 and shows the formation of the stream of descending cold fluid near that boundary.

The horizontal slice at $z = 1$, figure 5(a, b), shows the four streams crossing the mid-height plane. Between these streams the fluid moves inwards along the diagonals

of the cross-section. This is evidenced by the directional markers on some of the traces in figure 5 (*a*). The slice at $z = 0{\cdot}5$ (which plane does *not* coincide with the rotational axis of the vortex ring) clearly confirms the shape in horizontal plan of the stretched vortex ring in the upper half of the thermosyphon.

With respect to the form of the flow field, the photographs and their simulations show favourable agreement. A quantitative comparison is difficult since the three-dimensionality of the flow means that the particles may not remain illuminated for the duration of the exposure. This effect is evident in figure 4 (*a*) for example, in that very few of the traces actually exhibit the directional marker. A smaller time interval alleviates this effect but the accuracy of the comparison is adversely affected.

Despite the limited validity of making a quantitative comparison, one general area of discord between the photographs and the numerical simulations is evident in figure 4 (*c*) and figure 4 (*f*). The numerical simulation consistently over-estimates the magnitude of the fluid velocity near the boundaries of the cavity. The streamline tracing procedure uses linear interpolation between mesh points: this is clearly in error close to a stationary boundary.

The flow in each quarter of the cavity (delineated by the vertical planes of symmetry) is complex, and many streamlines were traced before an understanding of its form was obtained. If a streamline is followed from an arbitrary point, it executes a looping pattern between the upper and lower halves of the cavity as it alternates between the two stretched vortex rings. Once started in a particular quarter of the box, a streamline remains in that quarter. The basic form of the motion is revealed by the line in figure 6 which was chosen so that it entered one of the vortices close to one of the planes of symmetry. The particular line shown started from the point (0·01, 0·5001, 0·2) which is near the top of the $x = 0$ boundary and just in the quarter cavity ($x < 0{\cdot}5$, $y > 0{\cdot}5$). It enters the vortex adjacent to that boundary and spirals inwards to the centre of rotation, where it changes direction and follows a path towards the plane $x = 0{\cdot}5$. Near this plane it changes direction and moves out towards the $y = 1$ boundary and ascends into the upper half of the cavity to the centre of the vortex adjacent to that boundary. Fluid in the vortex adjacent to the $y = 1$ wall and in the same quarter of the cavity as the streamline in figure 6 returns to the vicinity of the $y = 0{\cdot}5$ plane by a similar path in the upper half of the thermosyphon.

Similar flow structures exist for the two-stream and six-stream flows. However, it is beyond the scope of this discussion to describe them in detail. Experimental verification of these configurations is shown in figure 7.

Figure 7 (*a*, *b*) shows the $x = 0{\cdot}5$ slice of a two-stream flow for $Ra \simeq 10^4$ in which the boundary between the streams is along the $x = y$ diagonal in the $z = 1$ plane. The slice has cut the edges of the ascending hot and descending cold streams which are centred near the $x = 0$, $y = 1$ and $x = 1$, $y = 0$ corners of the mid-height plane respectively.

Figure 7 (*c*, *d*) shows a similar slice for a six-stream flow. The distribution of the six streams is such that one pair of streams is centred on a diagonal of the mid-height plane. The other diagonal forms the boundaries between the remaining streams. An $x = 0{\cdot}5$ or $y = 0{\cdot}5$ slice always cuts one ascending and one descending stream. Bearing in mind the difference in Rayleigh numbers, the agreement in form is favourable. As remarked in § 5.1(*a*), the Rayleigh numbers 10^5 and $1{\cdot}65 \times 10^5$ are near a critical value when the flow field tends to be unstable. This is reflected by the asymmetry

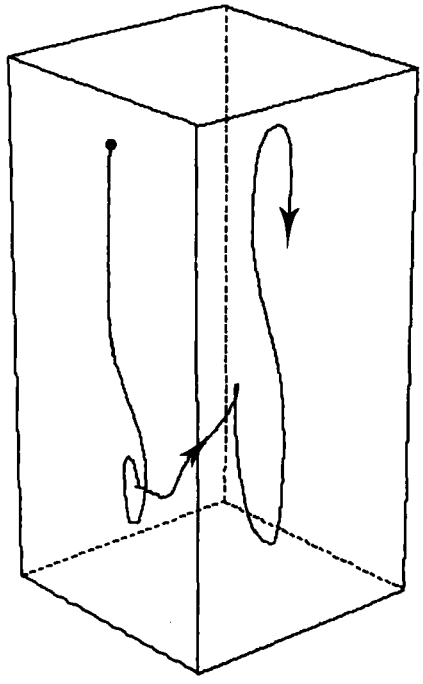

FIGURE 6. Streamline at $Ra = 10^5$ showing the coupling between the planes of symmetry.

in the positions of the centres of rotation in the photograph. In the experiment these centres drifted slowly with time.

5.2. *Heat transfer*

For each numerical solution, equations (8) and (9) were used to evaluate the Nusselt number. Plotting Nu against Ra gave a separate curve for each aspect ratio. Moreover, the data were insufficient to isolate sections of the curve pertaining to the different flow configurations. In the following correlation the Nusselt numbers for those values of Ra at which multiple flow configurations exist correspond to the configurations that convect the most heat.

Japikse *et al.* (1971) define an alternative Nusselt number,

$$Nu_d = h_f L/k, \tag{17}$$

where h_f is a film coefficient obtained by averaging the total heat flux over the area of the upper half of the vertical walls of the thermosyphon. Clearly

$$Nu_d = Nu/2h. \tag{18}$$

When Nu_d is plotted against t_{ct} ($= 2Ra/h$), as in figure 8, the effect of h is insignificant, to within the probable error of the Nu estimates, and for $Ra \geqslant 2 \times 10^4$. A least-squares fit of the data yields

$$Nu_d = 0{\cdot}035 t_{ct}^{0{\cdot}4} \tag{19}$$

or

$$Nu = 0{\cdot}092 h^{0{\cdot}6} Ra^{0{\cdot}4}. \tag{20}$$

This correlation is indicated in figure 8. A comparison with the model of Japikse *et al.* (1971) is an extrapolation since their model is valid only for $t_{ct} > 5 \times 10^5$. For $t_{ct} = 10^6$

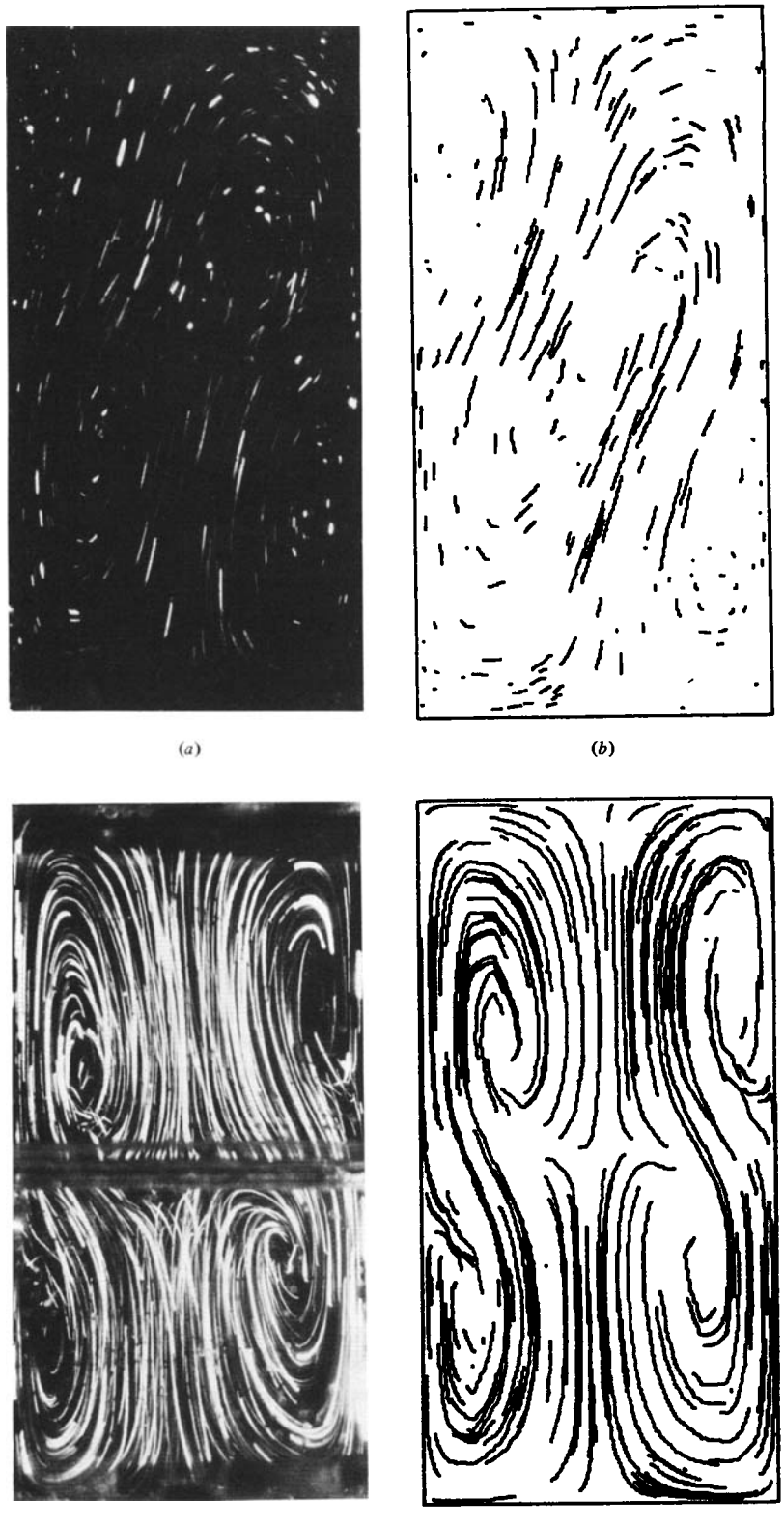

(a) (b)

(c) (d)

FIGURE 7. Flow field at $x = 0{\cdot}5$. (a) $Ra = 9 \times 10^3$ ($\Delta t = 5$ min). (b) Numerical simulation, $Ra = 10^4$ (two stream flow). (c) $Ra = 1{\cdot}65 \times 10^5$ ($\Delta t = 8$ min). (d) Numerical simulation, $Ra = 10^5$ (six stream flow).

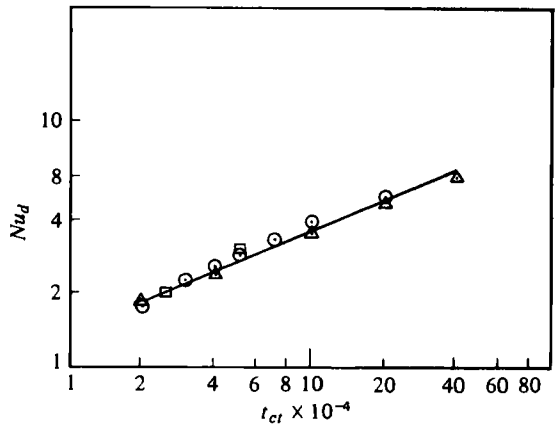

FIGURE 8. Numerical estimates of Nu_d for $t_{ct} \leqslant 4 \times 10^5$. △, $h = 1$; ⊙, $h = 2$; ⊡, $h = 4$. ——, equation (19).

equation (19) gives $Nu_d = 8{\cdot}8$, whereas an estimate from their figure 6 is $Nu_d = 7{\cdot}2$. Our estimate is 22 % higher which could be attributed to the fact that the numerical model has isothermal ends rather than the adiabatic ends assumed by Japikse *et al.* (1971).

The data for $t_{ct} < 2 \times 10^4$ are insufficient to determine in detail the dependence of Nu_d on h. However, the series solutions for $Ra = 0$ indicate that Nu is independent of h for $h \geqslant 2$ and the correlation (19) cannot be expected to hold as $Ra \to 0$.

6. Conclusions

A study, both numerical and experimental, has been made of the laminar flow in a closed thermosyphon of square cross-section. Excellent agreement has been obtained between the finite-difference solutions and the experimental visualizations for a flow which is not only fully three-dimensional but also exhibits a series of transitions as the Rayleigh number is increased. The numerical solutions for a high-Prandtl-number fluid have successfully identified a conduction regime with a weak toroidal flow and a convection regime in which an increasing number of individual streams cross the mid-height plane with increasing Ra. Three critical Rayleigh numbers for the transitions from toroidal to two-stream flow, two-stream to four-stream flow and four-stream to six-stream flow have been estimated. These critical values together with a tendency towards temporal instability when Ra is near a critical value were supported by the flow visualization study.

Apart from minor alignment features associated with the shape of the cross-section, the present results are in favourable agreement with previous observations for a thermosyphon of circular cross-section.

For $Ra < 10^3$, a series expression for the Nusselt number is valid. Numerical estimates of Nu for $10^4 \leqslant Ra \leqslant 10^5$ have been shown to follow a relationship that is similar in form to those developed for higher Ra by Japikse *et al.* (1971).

The research was supported in part by a grant to one of us (de Vahl Davis) from the Australian Research Grants Committee for which the authors are grateful.

REFERENCES

BOUSSINESQ, J. 1903 *Théorie Analytique de la Chaleur*, vol. 2, p. 172. Gauthier-Villars.

JAPIKSE, D., JALLOUK, P. A. & WINTER, E. R. F. 1971 Single-phase transport processes in the closed thermosyphon. *Int. J. Heat Mass Transfer* **14**, 869–887.

JAPIKSE, D. & WINTER, E. R. F. 1970 Heat transfer and flow in the closed thermosyphon. In *Heat Transfer* 1970, vol. 4, paper NC2. 9. Elsevier.

LARKIN, B. S. 1967 Heat transfer in a two-phase thermosyphon tube. *Canada Nat. Res. Counc. Rep.* no. 3, pp. 45–53.

MALLINSON, G. D. & DE VAHL DAVIS, G. 1973 The method of the false transient for the solution of coupled elliptic equations. *J. Comp. Phys.* **12**, 435–461.

MALLINSON, G. D. & DE VAHL DAVIS, G. 1977 Natural convection in a box: a numerical study. *J. Fluid Mech.* **83**, 1–31.

MALLINSON, G. D. & GRAHAM, A. D. 1974 Experimental visualisation of three dimensional natural convection. *Proc. 5th Aust. Conf. Hydraulics and Fluid Mech., Christchurch, N.Z.*, vol. 2, pp. 323–330.

OGALE, V. A. 1968 On the application of the semi-closed thermosyphon system to gas turbine blade cooling. Dr. Diss. Technological University Delft.